Commun. Comput. Phys.
doi: 10.4208/cicp.121114.210415a

Vol. **19**, No. 1, pp. 168-191
January 2016

Relaxation Schemes for the M_1 Model with Space-Dependent Flux: Application to Radiotherapy Dose Calculation

Teddy Pichard[1,2,*], Denise Aregba-Driollet[3], Stéphane Brull[3], Bruno Dubroca[1,3] and Martin Frank[2]

[1] *Centre Lasers Intenses et Applications, Université de Bordeaux, 351 cours de la libération, Talence, 33400,France.*
[2] *Mathematics division, Center for Computational Engineering Science, Rheinisch-Westfälische Technische Hochschule, Schinkelstrasse 2, Aachen, 52062, Germany.*
[3] *Institut de Mathématiques de Bordeaux, Université de Bordeaux, 351 cours de la libération, Talence, 33400, France.*

Received 12 November 2014; Accepted (in revised version) 21 April 2015

Abstract. Because of stability constraints, most numerical schemes applied to hyperbolic systems of equations turn out to be costly when the flux term is multiplied by some very large scalar. This problem emerges with the M_1 system of equations in the field of radiotherapy when considering heterogeneous media with very disparate densities. Additionally, the flux term of the M_1 system is non-linear, and in order for the model to be well-posed the numerical solution needs to fulfill conditions called realizability. In this paper, we propose a numerical method that overcomes the stability constraint and preserves the realizability property. For this purpose, we relax the M_1 system to obtain a linear flux term. Then we extend the stencil of the difference quotient to obtain stability. The scheme is applied to a radiotherapy dose calculation example.

AMS subject classifications: 82C40, 35L65, 65M25

Key words: Radiotherapy, Moments models, relaxation models, method of characteristics.

1 Introduction

The present work is devoted to the numerical solution of a moment system of equations, which describes the transport of electrons in tissues. The model finds application in the

*Corresponding author. *Email addresses:* pichard@celia.u-bordeaux1.fr (T. Pichard), denise.aregba@math.u-bordeaux1.fr (D. Aregba-Driollet), stephane.brull@math.u-bordeaux1.fr (S. Brull), bruno.dubroca@math.u-bordeaux1.fr (B. Dubroca), frank@mathcces.rwth-aachen.de (M. Frank)

field of radiotherapy dose calculation when considering low density media [11]:

$$\frac{1}{\rho(x)}\nabla_x.\psi^1(x,\epsilon)=\partial_\epsilon(S(\epsilon)\psi^0)(x,\epsilon), \tag{1.1a}$$

$$\frac{1}{\rho(x)}\nabla_x.\psi^2(x,\epsilon)=\partial_\epsilon(S(\epsilon)\psi^1)(x,\epsilon)-2T(\epsilon)\psi^1(x,\epsilon), \tag{1.1b}$$

where the unknowns $\psi^0\in\mathbb{R}$, $\psi^1\in\mathbb{R}^3$ and $\psi^2\in\mathbb{R}^{3\times3}$ depend on energy $\epsilon\in\mathbb{R}^+$ and position $x\in\mathbb{R}^3$. The stopping power $S>0$ and the transport coefficient $T\geq0$ are functions of ϵ characterizing the loss of energy and the deflection of the electrons during their transport. Finally, $\rho(x)>0$ is the density of the medium at point x. This equation is solved by marching backward in energy, i.e. we prescribe $\psi^0(\epsilon_{\max},x)=0$ and $\psi^1(\epsilon_{\max},x)=0_{\mathbb{R}^3}$ at initial energy $\epsilon_{\max}$ (which means that electrons have bounded energy) and we solve (1.1) from $\epsilon_{\max}$ to 0. This choice is motivated by two reasons. First, the system (1.1) is obtained from the following kinetic equation [11]

$$\frac{\Omega}{\rho(x)}.\nabla_x\psi(x,\epsilon,\Omega)=\partial_\epsilon(S(\epsilon)\psi)(x,\epsilon,\Omega)+T(\epsilon)\partial_\mu\left((1-\mu^2)\partial_\mu\psi\right)(x,\epsilon,\Omega), \tag{1.2}$$

by extracting moments (integrating over all $\Omega=(\mu,\sqrt{1-\mu^2}\cos\phi,\sqrt{1-\mu^2}\sin\phi)\in S^2$ gives (1.1a) and multiplying (1.2) by Ω and integrating over all $\Omega\in S^2$ gives (1.1b)). One realizes that the collision operator in (1.2) is backward parabolic in ϵ. Indeed it is ill-posed when working in the direction of increasing ϵ. Second, this choice is also consistent with the physics. Indeed the electrons only loses electrons in the medium. They are injected with a maximum energy which progressively decreases. In order to be consistent with both the underlying kinetic equation and the physics behind it, we always solve (1.1) from a maximum energy $\epsilon_{\max}$ to 0.

1.1 M_1 model

The system (1.1) is composed of 4 equations with 9 unknowns (scalar ψ^0, vector ψ^1 and symmetric matrix with known trace ψ^2). It is closed using the entropy minimization principle [19]:

We seek the function $\psi_M\geq0$ minimizing the Boltzmann entropy function

$$\mathcal{H}(f)=\int_{S^2}f(\Omega)\ln f(\Omega)d\Omega$$

under the constraint of realizing the moments of order 0 and 1, i.e.

$$\int_{S^2}f(\Omega)d\Omega=\psi^0,\quad \int_{S^2}\Omega f(\Omega)d\Omega=\psi^1.$$

We close the system (1.1) *by fixing ψ^2 as the 2nd order moment of ψ_M*

$$\psi^2=\int_{S^2}\Omega\Omega^T\psi_M(\Omega). \tag{1.3}$$

System (1.1) with this closure is called M_1 model. The M_1 model is closely related to some underlying kinetic model because the function ψ_M minimizing the Boltzmann entropy is known to be the most probable kinetic distribution function realizing the first two moments [5, 15]. In the standard case of $\rho = S = 1$, this choice of closure provides several desirable properties such as hyperbolicity of (1.1) and entropy dissipation [19].

Other choices are possible to close system (1.1). The P_N closure (for system of order N, see e.g. [17, 24]) is defined by choosing ψ_M as a polynomial function of Ω realizing the first moments. However, this choice does not guarantee the positivity of the underlying distribution function ψ_M (although the P_N closure was modified in [14] to enforce this property) and it is not as accurate as M_1 when studying beam-like distributions of particles.

Moment models are a good compromise between full kinetic models, precise but numerically costly, and diffusion models, not able to represent some physical phenomena. They are therefore often used in plasma physics (see e.g. [10, 20, 21] for application to the Vlasov-Fokker-Planck and Landau-Fokker-Planck equations) and in radiative transfer (see e.g. [9, 22]).

The M_1 model is valid under a condition on ψ^0 and ψ^1. Indeed, the M_1 closure exists only if there exists such a non-negative function ψ_M. This requirement is called realizability condition. A special attention is needed for this condition when developing numerical schemes for (1.1). We define the set $\mathcal{A}_1$ of realizable moments by

$$\left(\psi^0,\psi^1\right)\in\mathcal{A}_1 \;\Leftrightarrow\; \exists f\geq 0, \quad \text{s.t.} \quad \int_{S^2} f(\Omega)d\Omega=\psi^0, \quad \text{and} \quad \int_{S^2}\Omega f(\Omega)d\Omega=\psi^1. \tag{1.4}$$

Note that $\mathcal{A}_1$ is a convex cone. Numerical schemes applied to the system (1.1) need to preserve the realizability property.

For the M_1 model, the realizability property can be characterized by [16]

$$\mathcal{A}_1=\{(0,0_{\mathbb{R}^3})\}\cup\left\{(\psi^0,\psi^1)\in\mathbb{R}^{*+}\times\mathbb{R}^3 \;\text{ s.t. }\; \frac{|\psi^1|}{\psi^0}<1\right\}, \tag{1.5}$$

where $|\cdot|$ denotes the Euclidean norm.

If $(\psi^0,\psi^1)\in\mathcal{A}_1$ one can compute the closure. By geometrical considerations [18],

$$\psi^2=\psi^0\left(\frac{3\chi-1}{2}\frac{\psi^1}{|\psi^1|}\otimes\frac{\psi^1}{|\psi^1|}+\frac{1-\chi}{2}Id\right), \tag{1.6}$$

where χ is the Eddington factor and depends only on $|\psi^1|/\psi^0\in[0,1[$.

1.2 Problem statement

In radiotherapy, the studied electrons may be transported through strongly heterogeneous media, e.g. $\rho=1$ in water and $\rho=10^{-3}$ in air. Standard numerical schemes applied to (1.1) require a number of iterations of the order of $1/\min(\rho)$ (which can be very large),

which prevents these schemes from being usable for practical application. To see this, consider a one dimensional problem. In slab geometry, (1.1) can be reduced into

$$\frac{1}{\rho(x)}\partial_x\psi^1(x,\epsilon)=\partial_\epsilon(S(\epsilon)\psi^0)(x,\epsilon), \tag{1.7a}$$

$$\frac{1}{\rho(x)}\partial_x\psi^2(x,\epsilon)=\partial_\epsilon(S(\epsilon)\psi^1)(x,\epsilon)-2T(\epsilon)\psi^1(x,\epsilon), \tag{1.7b}$$

where ψ^i are now scalars and $x\in\mathbb{R}$. The previous closure in 1D simply reads

$$\psi^2=\chi(|\psi^1|/\psi^0). \tag{1.8}$$

To shorten notation, 1D system (1.7) is rewritten

$$\partial_\epsilon(S(\epsilon)\bar{\psi})=\frac{1}{\rho(x)}\partial_x\bar{F}(x,\epsilon)+T(\epsilon)L.\bar{\psi}, \tag{1.9}$$

where

$$\bar{\psi}=(\psi^0,\psi^1)^T,\quad \bar{F}=(\psi^1,\psi^2)^T \quad\text{and}\quad L=\begin{pmatrix}0&0\\0&2\end{pmatrix}.$$

The superscript $\bar{\cdot}$ refers to vectors.

As a first approach, we split the 1D system (1.7) and we use an HLL type scheme [7,13,26] to solve the homogeneous equation

$$\partial_\epsilon(S(\epsilon)\bar{\psi})-\frac{1}{\rho(x)}\partial_x\bar{F}(x,\epsilon)=0. \tag{1.10}$$

In the following, we describe the HLL scheme for (1.10) where the density $\rho(x)=\rho$ is constant. We extend afterward this approach for non-constant density. This numerical scheme is known to preserve the realizability domain from one step to the next one (see e.g. [3]). It is obtained by approximating the solution of the Riemann problem at each interface $x_{l+\frac{1}{2}}$. In the following, the subscript l refers to the position x and n to the energy ϵ.

First, we suppose $\rho(x)=\rho$ constant and $S(\epsilon)=S^n$ constant over $[\epsilon^{n+1}=\epsilon^n-\Delta\epsilon^n,\epsilon^n]$. Now suppose $\bar{\psi}(x,\epsilon^n)=\bar{\psi}_l^n$ and $\bar{F}(x,\epsilon^n)=\bar{F}_l^n$ for $x\in[x_l,x_{l+\frac{1}{2}}]$, and $\bar{\psi}(x,\epsilon^n)=\bar{\psi}_{l+1}^n$ and $\bar{F}(x,\epsilon^n)=\bar{F}_{l+1}^n$ for $x\in[x_{l+\frac{1}{2}},x_{l+1}]$. The discontinuity in $x_{l+\frac{1}{2}}$ produces waves that propagate with velocities c_j that are the eigenvalues of $\partial_{S\bar{\psi}}\bar{F}/\rho$. In the case of M_1 system, the velocities c_j are of norm inferior to $1/\rho S^n$ (see computations in [3]). Let us define the cone $\mathcal{C}_{l+\frac{1}{2}}^n$ (see Fig. 1)

$$\mathcal{C}_{l+\frac{1}{2}}^n=\left\{(x,\epsilon)\in\mathbb{R}\times\mathbb{R}^+,\ \text{s.t.}\ |x-x_{l+\frac{1}{2}}|\le\frac{|\epsilon-\epsilon^n|}{\rho S^n}\right\}.$$

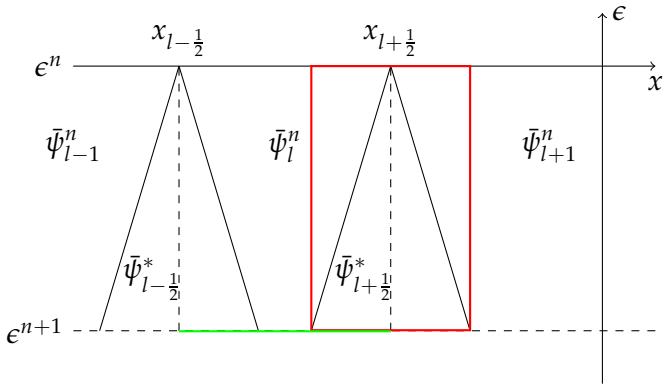

Figure 1: Configuration for the HLL solver.

We will approximate the value of $\bar{\psi}(x,\epsilon)$ inside the cone $\mathcal{C}^n_{l+\frac{1}{2}}$ by its average value

$$\bar{\psi}^*_{l+\frac{1}{2}} = \frac{1}{\Delta x}\int_{x_{l+\frac{1}{2}}-\frac{\Delta\epsilon^n}{\rho S^n}}^{x_{l+\frac{1}{2}}+\frac{\Delta\epsilon^n}{\rho S^n}} \bar{\psi}(\epsilon^{n+1},x)dx.$$

Note that as the wave speeds c_j are inferior to $1/\rho S^n$, the values of $\bar{\psi}$ out of the cone is constant respectively equal to $\bar{\psi}^n_l$ on the left and to $\bar{\psi}^n_{l+1}$ on the right.

To compute this average value, we integrate (1.10) over

$$\left[x_{l+\frac{1}{2}}-\frac{\Delta\epsilon^n}{\rho S^n},x_{l+\frac{1}{2}}+\frac{\Delta\epsilon^n}{\rho S^n}\right]\times[\epsilon^{n+1},\epsilon^n]$$

(in red on Fig. 1)

$$0=\frac{2\Delta\epsilon^n}{S^n\rho}\left[\frac{S^n}{2}(\bar{\psi}^n_l+\bar{\psi}^n_{l+1})-S^{n+1}\bar{\psi}^*_{l+\frac{1}{2}}\right]+\frac{\Delta\epsilon^n}{\rho}(\bar{F}^n_{l+1}-\bar{F}^n_l),$$

which gives

$$S^{n+1}\bar{\psi}^*_{l+\frac{1}{2}}=\frac{S^n}{2}(\bar{\psi}^n_l+\bar{\psi}^n_{l+1})+\frac{S^n}{2}(\bar{F}^n_{l+1}-\bar{F}^n_l).$$

Now to compute the result of the splitted operator $\bar{\psi}^{n+\frac{1}{2}}$ at new energy step, we integrate $S(\epsilon^{n+1})\bar{\psi}(x,\epsilon^{n+1})$ over $[x_{l-\frac{1}{2}},x_{l+\frac{1}{2}}]$ (in green on Fig. 1). Using the previous computations, this reads

$$\begin{aligned}S^{n+1}\bar{\psi}^{n+\frac{1}{2}}_l &= \frac{1}{\Delta x}\left(\frac{\Delta\epsilon^n}{S^n\rho}(S^{n+1}\psi^*_{l-\frac{1}{2}}+S^{n+1}\psi^*_{l+\frac{1}{2}})+\left(\Delta x-\frac{2\Delta\epsilon^n}{S^n\rho}\right)S^n\psi^n_l\right)\\ &= S^n\bar{\psi}^n_l+\frac{\Delta\epsilon^n}{\rho\Delta x}\left(\bar{G}^n_{l+\frac{1}{2}}-\bar{G}^n_{l-\frac{1}{2}}\right),\end{aligned}$$

with

$$\bar{G}^n_{l+\frac{1}{2}} = \frac{1}{2}\left(\bar{F}^n_{l+1} + \bar{F}^n_l + (\bar{\psi}^n_{l+1} - \bar{\psi}^n_l)\right). \tag{1.11}$$

Note that we can use the previous calculation as long as the waves produced in $x_{l-\frac{1}{2}}$ and $x_{l+\frac{1}{2}}$ do not cross each other, i.e. under the Courant Friedrichs Lewy (CFL) condition

$$\Delta\epsilon^n \leq S^n \left(\frac{1}{\rho\Delta x}\right)^{-1}. \tag{1.12}$$

In our case, the density ρ is heterogeneous. We approximate the density by a function $\rho = \rho_{l+\frac{1}{2}}$ constant over each interval $[x_l, x_{l+1}]$. Then the previous computation with this density ρ leads to write

$$S^{n+1}\bar{\psi}^{n+\frac{1}{2}}_l = S^n\bar{\psi}^n_l + \frac{\Delta\epsilon^n}{\Delta x}\left(\frac{\bar{G}^n_{l+\frac{1}{2}}}{\rho_{l+\frac{1}{2}}} - \frac{\bar{G}^n_{l-\frac{1}{2}}}{\rho_{l-\frac{1}{2}}}\right),$$

with the fluxes (1.11) and under the CFL condition

$$\Delta\epsilon^n \leq S^n \left(\frac{1}{2\Delta x}\max_l\left(\frac{1}{\rho_{l+\frac{1}{2}}} + \frac{1}{\rho_{l-\frac{1}{2}}}\right)\right)^{-1}. \tag{1.13}$$

Finally we add the influence of the source term. The scheme finally reads

$$S^{n+1}\bar{\psi}^{n+1}_l = \left[S^n\bar{\psi}^n_l + \frac{\Delta\epsilon^n}{\Delta x}\left(\frac{\bar{G}^n_{l+\frac{1}{2}}}{\rho_{l+\frac{1}{2}}} - \frac{\bar{G}^n_{l-\frac{1}{2}}}{\rho_{l-\frac{1}{2}}}\right) - \Delta\epsilon^n T^n L.\bar{\psi}^n_l\right], \tag{1.14}$$

which can be rewritten

$$\begin{aligned}
S^{n+1}\psi^{0^{n+1}}_l &= S^n\psi^{0^n}_l + \frac{\Delta\epsilon^n}{2\Delta x}\left(\frac{\psi^{0^n}_{l+1}}{\rho_{l+\frac{1}{2}}} - \psi^{0^n}_l\left(\frac{1}{\rho_{l+\frac{1}{2}}} + \frac{1}{\rho_{l-\frac{1}{2}}}\right) + \frac{\psi^{0^n}_{l-1}}{\rho_{l-\frac{1}{2}}}\right) \\
&\quad + \frac{\Delta\epsilon^n}{2\Delta x}\left(\frac{\psi^{1^n}_{l+1}}{\rho_{l+\frac{1}{2}}} + \psi^{1^n}_l\left(\frac{1}{\rho_{l+\frac{1}{2}}} - \frac{1}{\rho_{l-\frac{1}{2}}}\right) - \frac{\psi^{1^n}_{l-1}}{\rho_{l-\frac{1}{2}}}\right), \\
S^{n+1}\psi^{1^{n+1}}_l &= S^n\psi^{1^n}_l + \frac{\Delta\epsilon^n}{2\Delta x}\left(\frac{\psi^{1^n}_{l+1}}{\rho_{l+\frac{1}{2}}} - \psi^{1^n}_l\left(\frac{1}{\rho_{l+\frac{1}{2}}} + \frac{1}{\rho_{l-\frac{1}{2}}}\right) + \frac{\psi^{1^n}_{l-1}}{\rho_{l-\frac{1}{2}}}\right) - 2\Delta\epsilon^n T^n\psi^{1^n}_l \\
&\quad + \frac{\Delta\epsilon^n}{2\Delta x}\left(\frac{\psi^{2^n}_{l+1}}{\rho_{l+\frac{1}{2}}} + \psi^{2^n}_l\left(\frac{1}{\rho_{l+\frac{1}{2}}} - \frac{1}{\rho_{l-\frac{1}{2}}}\right) - \frac{\psi^{2^n}_{l-1}}{\rho_{l-\frac{1}{2}}}\right).
\end{aligned}$$

In the second equation, in order to assure that $\psi^{1^{n+1}}$ is defined using a positive combination of ψ^{1^n} (which is a common stability requirement), we fix the following CFL

condition which is slightly more restrictive than (1.13) (due to the source term $T(\epsilon)L.\bar{\psi}$)

$$\Delta\epsilon^n \leq S^n \left(\frac{1}{\min(\rho_{l+\frac{1}{2}})\Delta x} + 2T^n \right)^{-1}. \tag{1.15}$$

In practice, the density ρ is inhomogeneous and can have very strong variations. Then $\min(\rho_{l+\frac{1}{2}})$ might be very low, and the numerical scheme requires very small $\Delta\epsilon^n$.

This problem was investigated in [4] and solved by modifying the grid in one space dimension. The generalization to multi-dimensional (multi-D) problems was not straightforward, and introduced additional splitting errors. In the present paper, we propose a numerical approach ensuring the realizability that does not constrain the energy step, independent of the grid, and which works for multi-D problems. In Section 2, we describe the numerical approach which consists of two parts. First, we construct numerical schemes for linear hyperbolic equations with spatially varying flux that are unconditionally stable. Second, we use a relaxation model to approximate the M_1 model on which we can apply those schemes. The last section is devoted to the validation of the numerical approach on relevant test cases.

2 Numerical approach

We write the multi-D system (1.1) in the form

$$\partial_\epsilon(S(\epsilon)\bar{\psi}) = \frac{1}{\rho(x)}\nabla_x.\bar{\bar{F}}(x,\epsilon) + T(\epsilon)L.\bar{\psi}, \tag{2.1}$$

with

$$L = \begin{pmatrix} 0 & 0_{\mathbb{R}^3} \\ 0^T_{\mathbb{R}^3} & -2Id \end{pmatrix}.$$

Here $\bar{\psi} = (\psi^0, \psi^1)^T \in \mathbb{R}^4$ and $\bar{\bar{F}} = (\psi^1, \psi^2) \in \mathbb{R}^{3\times 4}$. The superscript $\bar{\cdot}$ refers to vectors of vectors, i.e. matrices. Note that the divergence operator $\nabla_x.(\cdot)$ is applied separately to each vector component $\psi^1 \in \mathbb{R}^3$ and $\psi^2_{i,:} \in \mathbb{R}^3$ composing $\bar{\bar{F}} = (\psi^1, \psi^2_{1,:}, \psi^2_{2,:}, \psi^2_{3,:})$.

In a first part, we propose a numerical scheme for hyperbolic equations with space-dependent fluxes not constrained by any CFL condition. In a second part, we present a method to apply it to M_1 system of equations using relaxation models.

2.1 Scheme for fast characteristics in 1D

As mentioned above, for a standard scheme the density ρ in front of the flux term might lead to a severe CFL restriction. We overcome this problem by stencil extensions, which rely on a re-interpretation of the basic upwind scheme. For the sake of simplicity we describe this approach first for the linear advection equation. Consider

$$\partial_t u + \frac{a}{\rho(x)}\partial_x u = 0, \tag{2.2}$$

with $a>0$ (the case $a<0$ can be treated similarly). First let ρ be constant. In a basic Finite Difference (FD) scheme, we write $u_l^0 := u(x_l,0)$ and we compute u_l^n that approximates $u(x_l,t^n)$. A scheme is obtained by defining u_l^{n+1} as a convex combination C of some u_l^n such that this definition is consistent with (2.2).

Using the method of characteristics, u is constant along the characteristic curves which yields

$$u_l^{n+1} \approx u(x_l,t^{n+1}) = u(y(\tau,t^{n+1},x_l),\tau) \quad \text{with} \quad y(\tau,t,x) = x+\frac{a}{\rho}(\tau-t). \tag{2.3}$$

2.1.1 Constant ρ, CFL: $\Delta t < \frac{\rho}{a}\Delta x$

The common approach is to impose that the characteristic curve starting at $(x_l,t^n+\Delta t)$ is in the cell $[x_{l-1},x_l]$ at time t^n (see Fig. 2), i.e.

$$x_l \geq y(t^n,t^n+\Delta t,x_l) = x_l+\frac{a}{\rho}(t^n-(t^n+\Delta t)) > x_{l-1},$$

which is equivalent to the common CFL condition $\Delta t < \frac{a}{\rho}\Delta x$. Thus it seems natural to use a convex combination C of the points u_{l-1}^n and u_l^n as the characteristic curves falls down between these two points at time t^n. This corresponds to approximating u using a linear reconstruction. Thus we obtain the standard upwind scheme

$$u_l^{n+1} = Cu^n = (1-\alpha)u_l^n+\alpha u_{l-1}^n, \quad \alpha = \frac{a\Delta t}{\rho\Delta x} \in [0,1[.$$

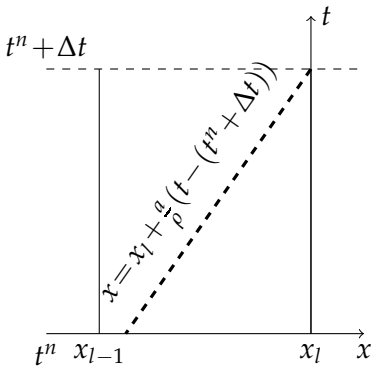

Figure 2: Characteristic curves when $\Delta t < \frac{a}{\rho}\Delta x$.

2.1.2 Constant ρ, CFL: $\Delta t < 2\frac{\rho}{a}\Delta x$

Now instead of the common CFL condition $\Delta t<\frac{\rho}{a}\Delta x$, let us impose the condition $\Delta t<2\frac{\rho}{a}\Delta x$. The characteristic curves can now cross into the next cell (see Fig. 3). Using again the

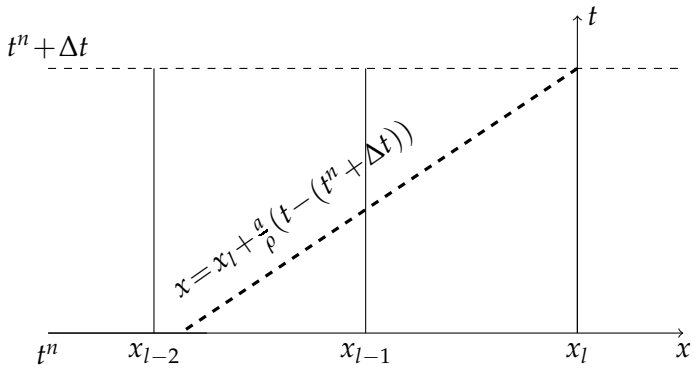

Figure 3: Characteristic curves when $\Delta t<2\frac{a}{\rho}\Delta x$.

method of characteristics, the foot of the characteristic curve is found between the points u^n_{l-1} and u^n_{l-2}. Then we define C by

$$u^{n+1}_l = Cu^n = (1-\alpha)u^n_{l-1}+\alpha u^n_{l-2}, \quad \alpha = \frac{a}{\rho}\frac{\Delta t}{\Delta x}-1 \in [0,1[.$$

2.1.3 Constant ρ, no CFL

We can generalize this to a time step Δt which is independent of Δx. Then the characteristic curves cross a certain number of cells k depending on Δt, Δx, a and ρ (see Fig. 4). More precisely, k is the only integer in the interval $]\frac{\rho}{a}\frac{\Delta t}{\Delta x},1+\frac{\rho}{a}\frac{\Delta t}{\Delta x}]$.

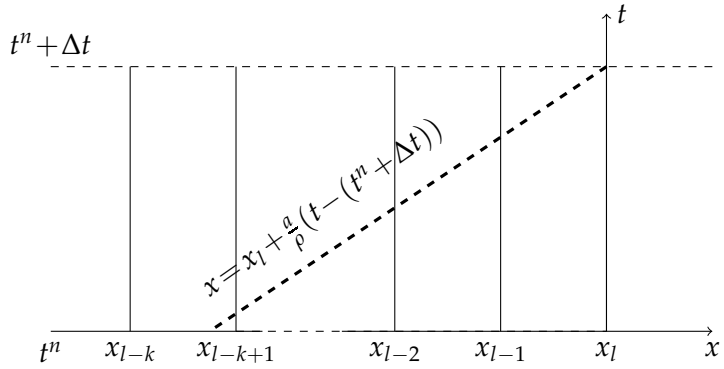

Figure 4: Characteristic curves when Δt is independent of Δx.

Then we define C as a convex combination of u^n_{l-k+1} and u^n_{l-k} and the scheme reads

$$u^{n+1}_l = Cu^n = (1-\alpha)u^n_{l-k+1}+\alpha u^n_{l-k}, \quad \alpha = \frac{a}{\rho}\frac{\Delta t}{\Delta x}-(k-1) \in [0,1[. \tag{2.4}$$

Remark 2.1. In the case of ρ uniform, integrating (2.2) over $[x_{l-\frac{1}{2}},x_{l+\frac{1}{2}}]\times[t^n,t^n+\Delta t]$ and approximating the solution u by a function constant in each cell $[x_{l-\frac{1}{2}},x_{l+\frac{1}{2}}]$ at time t^n leads to

$$0=\frac{u_l^{n+1}-u_l^n}{\Delta t}+\frac{a}{\rho}\frac{u_{l+\frac{1}{2}}-u_{l-\frac{1}{2}}}{\Delta x},$$

with

$$u_{l+\frac{1}{2}}=\frac{1}{\Delta t}\int_{t^n}^{t^n+\Delta t}u(x_{l+\frac{1}{2}},\tau)d\tau,\quad u_l^n=\frac{1}{\Delta x}\int_{x_{l-\frac{1}{2}}}^{x_{l+\frac{1}{2}}}u(y,t^n)dy.$$

Then using the method of characteristics to compute the fluxes $u^n_{l+\frac{1}{2}}$ leads to

$$u_{l+\frac{1}{2}}=\frac{\rho\Delta x}{a\Delta t}\sum_{i=0}^{k-2}u_i^n+\left(1-(k-1)\frac{\rho\Delta x}{a\Delta t}\right)u_{l-k+1}^n.$$

And the obtained numerical scheme is equivalent to (2.4). This means that the Finite Difference scheme (2.4) can also be interpreted as a Finite Volume scheme. This is not true when ρ is not constant.

2.1.4 Non-constant ρ, no CFL

Now we allow ρ to depend on x. We approximate ρ by a constant $\rho_{l+\frac{1}{2}}$ in each interval $[x_l,x_{l+1}]$. In that case, we need to compute the point x_c which the characteristic that goes through $(x_l,t^n+\Delta t)$ reaches at time t^n (see Fig. 5). Similar to above, one finds the number of crossed cells k_l by using the conditions

$$\sum_{i=1}^{k_l-1}\frac{\rho_{l+\frac{1}{2}-i}}{a}\Delta x\le\Delta t\le\sum_{i=1}^{k_l}\frac{\rho_{l+\frac{1}{2}-i}}{a}\Delta x. \tag{2.5}$$

Then

$$x_c=x_{l-k_l+1}-c,\quad\text{where}\quad c=d\frac{a}{\rho_{l+\frac{1}{2}-k_l}},\quad d=\Delta t-\sum_{i=1}^{k_l-1}\frac{\Delta x\rho_{l+\frac{1}{2}-i}}{a}.$$

Finally we can compute u_l^{n+1} by interpolation to obtain the following FD scheme

$$u_l^{n+1}=(1-\alpha)u_{l-k_l+1}^n+\alpha u_{l-k_l}^n, \tag{2.6a}$$

where

$$\alpha=\frac{c}{\Delta x}=\frac{\Delta t}{\Delta x}-\sum_{i=1}^{k_l}\frac{\rho_{l+\frac{1}{2}-i}}{a}\in[0,1[. \tag{2.6b}$$

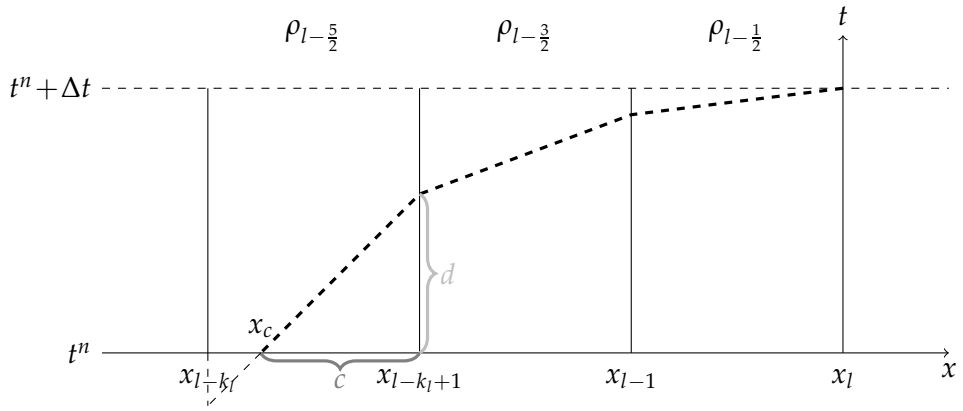

Figure 5: Configuration for CFL-free Finite Difference schemes for $k_l=3$.

Remark 2.2 (Properties of the scheme)**.**

- If the characteristic curves do not cross more than one cell, this scheme is equivalent to the original upwind scheme with the common CFL condition.
- The consistency error is $\mathcal{O}(\Delta x)$. So it is of order 1 in space and time.
- The FD scheme is linear with positive coefficients and whose sum is equal to 1. So it is monotone and therefore Total Variation (TV) stable.
- There are no stability restrictions on the scheme, so it is more stable than the common upwind scheme. This allows us to use a bigger time step. But one should keep in mind that the precision obtained when extending the stencil is lower as the one obtained using the common CFL restriction.

Remark 2.3. This method is closely related to the semi-lagrangian approach (see e.g. [12, 25]). With this method, one would compute the value of u_l^{n+1} by solving a transport equation in a Lagrangian framework. Then the obtained solution is projected on the Eulerian grid by using polynomial reconstruction. This correspond in our framework to following the characteristic curves. In the semi-lagrangian framework, ENO-WENO reconstruction are often used to improve the order of accuracy of the numerical scheme. Similar methods could also be used with our relaxation approach.

2.2 Extension to multi-D

We study the linear advection equation

$$\partial_t u+\frac{1}{\rho(x)}a.\nabla_x u=0, \tag{2.7}$$

where $a \in \mathbb{R}^n$ is a vector and u depends on $x \in \mathbb{R}^n$ and $t \in \mathbb{R}^+$.

For our purposes and in order to simplify the notations, we focus on the two dimensional problem but the method can easily be extended to higher dimensional problems.

Given a cell center X_{lm}, it is straightforward to find the origin X_c of the characteristic which passes through X_{lm} at time $t^n+\Delta t$ (cf. Fig. 6). We can then define a Finite Difference scheme by approximating the value of $u_h(X_c,t^n)$ using the values $u_h(\cdot,t^n)$ at the nearest cell centers $X_{l',m'}$ around $X_c=(X,Y)$

$$\begin{aligned} u_{l,m}^{n+1} &= u_h(X_{l,m},t^n+\Delta t) = u_h(X_c,t^n) \\ &\approx \sum_{i=0}^{1}\sum_{j=0}^{1} \frac{|X-x_{l'+i}|}{|x_{l'+1}-x_{l'}|}\frac{|Y-y_{m'+j}|}{|y_{m'+1}-y_{m'}|} u_{l'+i,m'+j}^n, \end{aligned} \tag{2.8}$$

if $X_c \in [x_{l'},x_{l'+1}]\times[y_{m'},y_{m'+1}]$.

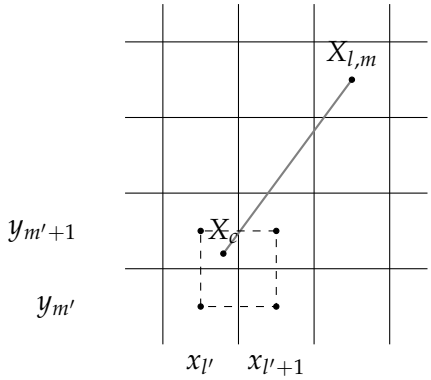

Figure 6: Characteristic for Finite Difference scheme in two dimensions.

2.3 Relaxation schemes for moment equations

The method presented in the last section cannot be directly applied to our problem as Eq. (2.1) has a non-linear flux. In order to use the previous method, we use a relaxation approximation of the 1D system (1.7) (afterward called AN after Aregba-Driollet and Natalini [1,2]) described in [23, 1] for hyperbolic systems of equations and completed for parabolic systems in [8, 2]. Special focus will be put on the preservation of the realizability domain. The extension to multi-D afterwards is straightforward.

2.3.1 Principle

We recall the principle of AN relaxation for 1D problems. Let us choose J speeds $(\lambda_j)_{j=1,\cdots,J} \in \mathbb{R}^J$. We associate to them a set of J moment vectors $\bar{\bar{f}}^\tau = \left(\bar{f}_j^\tau\right)_{j=1,\cdots,J} \in \mathbb{R}^{J\times 2}$ depending on a relaxation parameter τ and a set of Maxwellians $\bar{\bar{M}}^\tau = \left(\bar{M}_j^\tau\right)_{j=1,\cdots,J} \in \mathbb{R}^{J\times 2}$.

The Maxwellians are linked to the original moment vectors using a linear form P from $\mathbb{R}^{J\times 2}$ to $\mathbb{R}^2$ so that

$$P.\bar{\bar{M}}^\tau=\bar{\psi} \quad \text{and} \quad P.\Lambda.\bar{\bar{M}}^\tau=F(\bar{\psi}) \tag{2.9}$$

with $\Lambda=\text{Diag}(\lambda_j Id_{\mathbb{R}^{2\times 2}})$.

The following system of equations is a relaxation system for (1.9)

$$\rho\partial_\epsilon(S\bar{f}_j^\tau)-\lambda_j\partial_x\bar{f}_j^\tau+\rho TL.\bar{f}_j^\tau=\frac{1}{\tau}\left(\bar{M}_j^\tau(P.\bar{\bar{f}}^\tau)-\bar{f}_j^\tau\right), \quad 1\le j\le J. \tag{2.10}$$

The solution $\bar{\bar{f}}^0$ of the limit problem ($\tau\to 0$) corresponds to the desired solution of the original system (1.9). Formally, multiplying (2.10) by τ and $\tau\to 0$ leads to

$$\bar{M}_j^0(P.\bar{\bar{f}}^0)=\bar{f}_j^0.$$

Then replacing $\bar{f}_j^0$ by $\bar{M}_j^0$ in (2.10) and multiplying it on the left by P yields

$$\rho\partial_\epsilon(SP.\bar{\bar{M}}^0)-\partial_x(P.\Lambda.\bar{\bar{M}}^0)+\rho TL.(P.\bar{\bar{M}}^0)=0,$$

which is exactly (1.9).

As we only want to solve the limit system for $\tau\to 0$, the index τ is removed in the rest of this paper. The upper index n now refers to energy step ϵ^n, first lower index j to relaxation speed λ_j and second lower index l to position x_l. Note that the spatial fluxes of the relaxed system are linear even if the ones from the original system are not.

It is a well-known stability requirement [23, 6, 2] that all eigenvalues of $\partial_{S\bar{\psi}}\bar{F}(\bar{\psi})/\rho$ have to be bounded by the extremal relaxation speed, i.e.

$$\text{Spectrum}\left(\partial_{S\bar{\psi}}\frac{\bar{F}(\bar{\psi})}{\rho}\right)\subset\left[\min_j\frac{\lambda_j}{S\rho},\max_j\frac{\lambda_j}{S\rho}\right]. \tag{2.11}$$

In the 1D case, we choose two directions of relaxation ($J=2$) such that $-\lambda_1=\lambda_2=\lambda$ and we fix $P=(1,1)$. As the absolute values of the eigenvalues of $\partial_{S\bar{\psi}}\bar{F}(\bar{\psi})/\rho$ are less than $1/S\rho$ (see computations in [3]), we choose $\lambda=1$. This choice of speeds Λ and of P leads to write the Maxwellians

$$\bar{M}_1=\frac{\bar{\psi}-\bar{F}(\bar{\psi})}{2}, \quad \bar{M}_2=\frac{\bar{\psi}+\bar{F}(\bar{\psi})}{2}.$$

Note that applying the upwind discretization (with the CFL condition (1.15)) to the relaxed system (2.10) with this choice of parameters is equivalent to the HLL type scheme (1.14), (1.11) (see e.g. [7]). In practice, the solution of (1.9) is obtained by initializing $\bar{f}_1^0:=\bar{M}_1^0$ and $\bar{f}_2^0:=\bar{M}_2^0$ at the energy step ϵ^0, and then the relaxed system is solved using a splitting method:

- We define intermediate states $f_j^{n+\frac{1}{2}}$ by solving the equations without the relaxation terms

$$\partial_\epsilon(S\bar{f}_j)-\frac{\lambda_j}{\rho}\partial_x\bar{f}_j+TL.\bar{f}_j=0,\quad 1\leq j\leq 2. \tag{2.12}$$

  We discretize the term $L.\bar{f}_j$ implicitly (this choice is explained in the following). The spatial derivative is approximated by the finite difference formula (2.6) which leads to

$$S^{n+1}\bar{f}_{1_l}^{n+\frac{1}{2}}=S^n(C_1\bar{f}_1^{\,n})_l+\Delta\epsilon^n T^{n+1}L.\bar{f}_{1_l}^{n+\frac{1}{2}}, \tag{2.13a}$$

$$S^{n+1}\bar{f}_{2_l}^{n+\frac{1}{2}}=S^n(C_2\bar{f}_2^{\,n})_l+\Delta\epsilon^n T^{n+1}L.\bar{f}_{2_l}^{n+\frac{1}{2}}, \tag{2.13b}$$

  where $C_j\bar{f}_j^{\,n}$ is a convex combination of values of $\bar{f}_j^{\,n}$ (see Remarks 2.5 and 2.8).

- Then the solution is corrected by solving the rest of the equation, which, for $\tau\to 0$, corresponds to taking $\bar{M}_1^{n+1}:=\bar{f}_1^{n+\frac{1}{2}}$ and $\bar{M}_2^{n+1}:=\bar{f}_2^{n+\frac{1}{2}}$.

- The solution at new energy is computed as

$$\bar{\psi}^{n+1}:=\bar{M}_1^{n+1}+\bar{M}_2^{n+1}, \tag{2.14}$$

  as prescribed by the consistency condition (2.9) and considering $\bar{M}_1^{n+1}$ and $\bar{M}_2^{n+1}$ at new energy step.

Remark 2.4 (Properties of the approach)**.**

- The advantage of solving the relaxed system (2.10) instead of the original one (1.7) is that the relaxed system has a linear spatial flux $\frac{\lambda}{\rho}\partial_x\bar{f}_j^{\tau}$. So we can apply the scheme presented in the previous section to it.

- The drawback of this is that we need to solve twice more equations (or J times more equations if we choose J speeds).

2.3.2 Realizability

This method preserves the realizability property from an energy step to the next one:

Proposition 2.1. If for all l, we have $\bar{\psi}_l^n\in\mathcal{A}_1$ at energy step ϵ^n then the solution $\bar{\psi}_l^{n+1}$ obtained by solving the relaxed system (2.10) with the scheme (2.13) is also in $\mathcal{A}_1$ at energy step ϵ^{n+1} for all l.

Proof. The realizability of $\bar{\psi}^{n+1}$ is obtained via (2.14) through the realizability of $\bar{M}_1^{n+1}$, $\bar{M}_2^{n+1}$. In the first step, we show that $\bar{f}_1^0$ and $\bar{f}_2^0$ are realizable at initial energy ϵ^0. Second, we show by induction that $\bar{f}_1^{n+\frac{1}{2}}$ and $\bar{f}_2^{n+\frac{1}{2}}$ are realizable at the new energy step. Finally we conclude the realizability of $\bar{\psi}^{n+1}$.

1. We initialize $\bar{f}_1^0=\bar{M}_1^0=(\bar{\psi}^0+\bar{F}(\bar{\psi})^0)/2$ (respectively $\bar{f}_2^0=\bar{M}_2^0=(\bar{\psi}^0-\bar{F}(\bar{\psi})^0)/2$). Now suppose that $\bar{\psi}^0\in\mathcal{A}_1$, which means

$$\exists g\geq 0 \quad \text{s.t.} \quad \int_{-1}^{+1}(1,\mu)^T g d\mu=\bar{\psi}^0.$$

Since $\mu\in[-1,+1]$, we have $(1\pm\mu)g\geq 0$. We compute the moments of this function

$$\int_{-1}^{+1}(1,\mu)^T\frac{(1\pm\mu)g}{2}d\mu=\frac{\bar{\psi}^0\pm\bar{F}(\bar{\psi})^0}{2},$$

so $\bar{f}_1{}^0=(\bar{\psi}^0+\bar{F}(\bar{\psi})^0)/2\in\mathcal{A}_1$ and analogously $\bar{f}_2{}^0\in\mathcal{A}_1$.

2. Now let us prove that if for all l, $\bar{f}_{1l}{}^n\in\mathcal{A}_1$ then $\bar{f}_{1l}{}^{n+\frac{1}{2}}\in\mathcal{A}_1$. Based on $\bar{\psi}^n\in\mathcal{A}_1$, we construct a realizable vector $\bar{f}_1^n=\bar{M}_1^n=(\bar{\psi}^n+\bar{F}(\bar{\psi})^n)/2\in\mathcal{A}_1$ as in the first part of the proof. We solve (2.10) by splitting as described above. In the implicit energy step for the system without relaxations terms we need to solve

$$A.\bar{f}_{1l}{}^{n+\frac{1}{2}}=S^n(C_1\bar{f}_1{}^n)_l, \tag{2.15}$$

where

$$A=\begin{pmatrix}S^{n+1} & 0\\ 0 & S^{n+1}+2\Delta\epsilon^n T^{n+1}\end{pmatrix} \quad \text{and} \quad A^{-1}=\begin{pmatrix}1/S^{n+1} & 0\\ 0 & 1/(S^{n+1}+2\Delta\epsilon^n T^{n+1})\end{pmatrix}.$$

The right hand side of (2.15) is realizable, because $S^nC_1\bar{f}_1^n$ is a positive combination of realizable moments. Remark that the operator C_1 is related to the spatial component, i.e. it sums over several l, while the matrix A is related to the moment order, it impacts separately the zero-th and first order moments of a moment vector $\bar{f}_{1l}{}^n=(f_{1l}{}^{n0},f_{1l}{}^{n1})$. Obviously those operators are independent and commute. To simplify the notations in the rest of the proof, we write

$$\bar{g}=S^n(C_1\bar{f}_1^n)_l\in\mathcal{A}_1.$$

Then $\bar{g}=(g^0,g^1)$, where $g^0=S^n(C_1\bar{f}_1^n)_l^0$ and $g^1=S^n(C_1\bar{f}_1^n)_l^1$ correspond to a zero-th and first order moment. Using the characterization (1.5), $\bar{g}\in\mathcal{A}_1$ means that

$$\left|g^1\right|\leq g^0.$$

Since $1/S^{n+1}\geq 1/(S^{n+1}+2\Delta\epsilon^n T^{n+1})$, then

$$\left|(A^{-1}.g)^1\right|=\left|\frac{g^1}{S^{n+1}+2\Delta\epsilon^n T^{n+1}}\right|\leq\frac{g^0}{S^n}=(A^{-1}.g)^0.$$

Therefore, according to the characterization (1.5), $\bar{f}_{1_l}^{n+\frac{1}{2}} = A^{-1}.\bar{g} = S^n(A^{-1}.C_1\bar{f}_1^n)_l \in \mathcal{A}_1$, then $\bar{M}_{1_l}^{n+1} := \bar{f}_{1_l}^{n+\frac{1}{2}} \in \mathcal{A}_1$. And the result follows by (2.14).

The same result is true for $\bar{f}_2$. Then $\bar{M}_{1_l}^{n+1} = \bar{f}_{1_l}^{n+\frac{1}{2}} \in \mathcal{A}_1$ and $\bar{M}_{2_l}^{n+1} = \bar{f}_{2_l}^{n+\frac{1}{2}} \in \mathcal{A}_1$. We eventually obtain $\bar{\psi}_l^{n+1} \in \mathcal{A}_1$ by (2.14).

The proof is complete. □

2.3.3 Multi-dimensional case

As in 1D, we choose $\{\bar{\lambda}_j\}_{\{j=1,\cdots,J\}} \in \mathbb{R}^3$ (in 3D), which in this case are vectors instead of scalars. The 1D method (and also Proposition 2.1) did not use any 1D argument. One can rewrite the previous method with vectors $\bar{\lambda}_j$ instead of scalars. Then the method for solving the system (1.1) reads:

- At each energy step, we initialize $\bar{f}_j^n := \bar{M}_j^n$, where $\bar{M}_j^n$ solves

$$\sum_{j=1}^{J} \bar{M}_j^n = \bar{\psi}^n \in \mathbb{R}^4, \quad \sum_{j=1}^{J} \bar{\lambda}_j \otimes \bar{M}_j^n = \bar{F}^n \in \mathbb{R}^{3\times 4}, \tag{2.16}$$

  where $\otimes$ denotes tensorial product.

- Then we compute $\bar{f}_j^{n+\frac{1}{2}}$ for each $1 \le j \le J$ by solving the equations without relaxation terms

$$\partial_\epsilon(S\bar{f}_j) - \frac{\lambda_j}{\rho}.\nabla_x \bar{f}_j + L.\bar{f}_j = 0, \quad 1 \le j \le J, \tag{2.17}$$

  using the numerical scheme

$$S^{n+1}\bar{f}_{j_l}^{n+\frac{1}{2}} = S^n C_j \bar{f}_j^n + \Delta\epsilon^n \rho L.\bar{f}_j^{n+\frac{1}{2}}, \tag{2.18}$$

  where $C_j\bar{f}_j^n$ is a convex combination (2.8) of some $\bar{f}_{j_l}^n$.

- We update $\bar{M}_j^{n+1} := \bar{f}_j^{n+\frac{1}{2}}$ and finally $\bar{\psi}^{n+1} := \sum_{j=1}^{J} \bar{M}_j^{n+1}$.

Similarly Proposition 2.1 can be generalized to higher dimensions:

Proposition 2.2. If for all l, we have $\bar{\psi}_l^n \in \mathcal{A}_1$ at energy step ϵ^n then the solution $\bar{\psi}_l^{n+1}$ obtained by solving the relaxed system using the scheme (2.18) is also in $\mathcal{A}_1$ at energy step ϵ^{n+1} for all l.

2.4 Application to M_1 equations

Applying the FD scheme to the relaxed system (2.10) gives

$$C_1\bar{f}_{1l}^{\,n}=\alpha_l^+\bar{f}_{1l-k_l^+}^{\,n}+(1-\alpha_l^+)\bar{f}_{1l-k_l^++1}^{\,n}, \tag{2.19a}$$

$$C_2\bar{f}_{2l}^{\,n}=\alpha_l^-\bar{f}_{2l+k_l^-}^{\,n}+(1-\alpha_l^-)\bar{f}_{2l+k_l^--1}^{\,n}, \tag{2.19b}$$

with

$$\alpha_l^+=\frac{\Delta\epsilon^n}{S^n\rho_{l-k_l^++\frac{1}{2}}\Delta x}-\sum_{i=1}^{k_l^+-1}\frac{\rho_{l-i+\frac{1}{2}}}{\rho_{l-k_l^++\frac{1}{2}}}, \tag{2.20a}$$

$$\alpha_l^-=\frac{\Delta\epsilon^n}{S^n\rho_{l+k_l^--\frac{1}{2}}\Delta x}-\sum_{i=1}^{k_l^--1}\frac{\rho_{l+i-\frac{1}{2}}}{\rho_{l+k_l^--\frac{1}{2}}}, \tag{2.20b}$$

and $k_{l+\frac{1}{2}}^{\pm}$ defined by

$$\sum_{i=1}^{k_l^+-1}\rho_{l-i+\frac{1}{2}}S^n\Delta x\le\Delta\epsilon^n\le\sum_{i=1}^{k_l^+}\rho_{l-i+\frac{1}{2}}S^n\Delta x, \tag{2.21a}$$

$$\sum_{i=1}^{k_l^--1}\rho_{l+i-\frac{1}{2}}S^n\Delta x\le\Delta\epsilon^n\le\sum_{i=1}^{k_l^-}\rho_{l+i-\frac{1}{2}}S^n\Delta x. \tag{2.21b}$$

Remark 2.5. Using (2.21) in (2.20) leads to $\alpha_l^{\pm}\in[0,1[$. Then C_1 and C_2 are indeed convex combinations.

Remark 2.6. If we restrict the energy step $\Delta\epsilon$ using the CFL condition (1.15) then our approach is equivalent to the HLL type scheme (1.14), (1.11). Indeed we found in Section 2.1 that if the characteristic curves did not cross more than one cell the scheme (2.6) was upwind scheme. And solving the relaxed problem (2.10) with an upwind scheme is equivalent to solving the original problem with the HLL type scheme (1.14), (1.11). Our approach generalizes HLL scheme to the case of large $\Delta\epsilon$.

For the multi-D problem, we relax (2.1) in three different ways. We first choose the directions of relaxations $\bar{\lambda}_j$. From those, we propose a simple definition of the Maxwellians $\bar{M}_j^{\tau}$ that satisfy the consistency condition (2.16). Note that Proposition (2.2) requires realizable Maxwellians. As we know that $\bar{f}+\bar{\bar{F}}.V$ is realizable for any $V\in S^2$, we simply choose the Maxwellians proportional to $\bar{f}+\bar{\bar{F}}.\frac{\bar{\lambda}_j}{|\bar{\lambda}_j|}$. Finally we choose the norm of the velocities $|\bar{\lambda}_j|$ so that the defined Maxwellians satisfy the consistency condition (2.16). We simply choose:

- "Cartesian relaxation"

$$\text{Relaxation directions} \quad \bar{\lambda_1}=(2,0), \quad \bar{\lambda_2}=(-2,0), \quad \bar{\lambda_3}=(0,2), \quad \bar{\lambda_4}=(0,-2), \tag{2.22a}$$

$$\text{Associated Maxwellians} \quad \bar{M_i}=\frac{1}{4}\left(\bar{\psi}+\frac{\bar{\lambda_i}}{|\bar{\lambda_i}|}.\bar{\bar{F}}\right); \tag{2.22b}$$

- "Diagonal relaxation"

$$\text{Relaxation directions} \quad \bar{\lambda_1}=\frac{1}{\sqrt{2}}(2,2), \quad \bar{\lambda_2}=\frac{1}{\sqrt{2}}(-2,2),$$
$$\bar{\lambda_3}=\frac{1}{\sqrt{2}}(-2,-2), \quad \bar{\lambda_4}=\frac{1}{\sqrt{2}}(2,-2), \tag{2.23a}$$

$$\text{Associated Maxwellians} \quad \bar{M_i}=\frac{1}{4}\left(\bar{\psi}+\frac{\bar{\lambda_i}}{|\bar{\lambda_i}|}.\bar{\bar{F}}\right); \tag{2.23b}$$

- "Star relaxation"

$$\text{Relaxation directions} \quad \bar{\lambda_1}=(4,0), \quad \bar{\lambda_2}=(0,4), \quad \bar{\lambda_3}=(-4,0), \quad \bar{\lambda_4}=(0,-4),$$
$$\bar{\lambda_5}=\frac{1}{\sqrt{2}}(4,4), \quad \bar{\lambda_6}=\frac{1}{\sqrt{2}}(-4,4), \tag{2.24a}$$
$$\bar{\lambda_7}=\frac{1}{\sqrt{2}}(-4,-4), \quad \bar{\lambda_8}=\frac{1}{\sqrt{2}}(4,-4),$$

$$\text{Associated Maxwellians} \quad \bar{M_i}=\frac{1}{8}\left(\bar{\psi}+\frac{\bar{\lambda_i}}{|\bar{\lambda_i}|}.\bar{\bar{F}}\right). \tag{2.24b}$$

Simple computation leads to show that the Maxwellians are realizable and that they satisfy the consistency condition (2.9).

Remark 2.7. When the number of directions J is equal to the number of unknowns (in 2D $\bar{\psi}$ is composed of 3 components), and when the directions are fixed, then the Maxwellians are uniquely defined as a function of $\bar{\psi}$, $\bar{\bar{F}}$ and of the $\bar{\lambda_i}$. Here, there are more directions in each set (4 in the cartesian and diagonal sets and 8 in the star set) than unknowns, so other choices of Maxwellians may be used.

Remark 2.8. All of these schemes are defined using convex combinations. So Propositions 2.1 and 2.2 hold.

3 Numerical results

We study several test cases from radiotherapy dose calculation. We use physical values for stopping power and transport coefficient for electrons as described in [11]. The

function of interest is the dose defined by

$$D(x)=\int_0^{+\infty} S(\epsilon)\psi^0(x,\epsilon)d\epsilon. \tag{3.1}$$

In the test cases, the dose is normalized by the maximum dose. This normalized dose, called percentage depth dose (PDD) in the field of medical physics, is independent of the quantity of particles transported (which is arbitrary here), it depends only on their distribution.

3.1 1D heterogeneous medium

The spatial domain is 12 cm long, uniformly meshed with 1200 cells. It is composed of 2 cm wide slabs of homogeneous media, alternatively air ($\rho_{air}=10^{-3}$) and water ($\rho_{water}=1$), the first slab being air.

Incoming beams are prescribed as boundary conditions. The injected electrons are modeled as Gaussians in energy ϵ centered around the energy of the electron beam $\epsilon_0 = 10MeV$

$$(\psi^0,\psi^1)(x_b,\epsilon)=(\delta,0) \quad \text{if no beam enters in the medium from the end } x_b,$$
$$(\psi^0,\psi^1)(x_b,\epsilon)=K\alpha_\mu \exp\left(-\frac{1}{2}\left(\frac{\epsilon_0-\epsilon}{\alpha_\epsilon\epsilon_0}\right)^2\right), \quad \text{otherwise,}$$

where K is a numerical constant fixed at 10^{10} and $\delta=10^{-20}$ is a small numerical constant used to avoid divisions by 0. When applying the $\psi^0=\delta$ condition, we make sure that the beam from the other end is entirely dissipated in the medium. The initial distribution at $\epsilon_{max}=1.5\epsilon_0$ is zero. And $\alpha_\mu=(1,\frac{\psi^1}{\psi^0})=(1,0.98)$. Note that $\frac{\psi^1}{\psi^0}$ characterizes the "peakedness" of the beam ($\frac{\psi^1}{\psi^0}=\pm 1$ for a Dirac distribution in angle and $\frac{\psi^1}{\psi^0}=0$ for an isotropic distribution). We fix $\alpha_\epsilon=0.05$. With those parameters, the prescribed moment vector on the boundary is realizable.

First, we use a fine energy steps

$$\Delta\epsilon^n_{HLL}=0.95S^n\left(\frac{1}{\rho_{air}\Delta x}+2T^n\right)^{-1}. \tag{3.2}$$

With these parameters, the scheme presented in the previous section is equivalent to the HLL scheme (1.14, 1.11, 1.15). Second, we use a coarse energy step

$$\Delta\epsilon^n_{FD}=0.95S^n\left(\frac{1}{\rho_{water}\Delta x}+2T^n\right)^{-1}. \tag{3.3}$$

With these parameters, the stencils are extended only in air. The results obtained with the fine energy steps are expected to be more precise and are therefore considered as

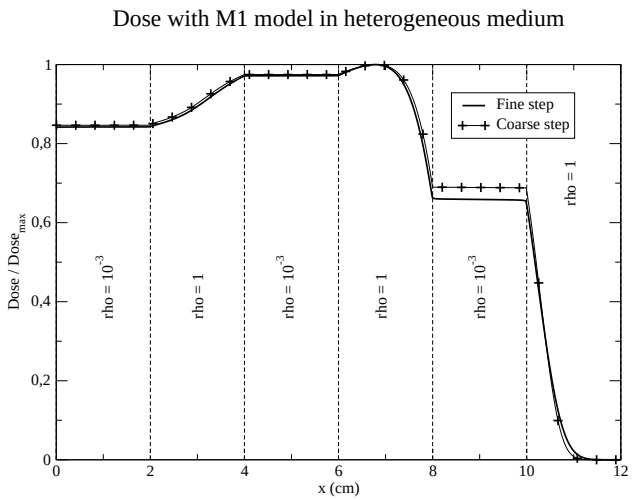

Figure 7: Dose with M_1 model for the simple beam test case in 1D heterogeneous medium with fine (equivalent to HLL scheme) and coarse $\Delta\epsilon$ (using FD schemes).

Table 1: Computation times for the 1D heterogeneous case with the different schemes.

energy step $\Delta\epsilon^n$	computation times	number of energy steps
fine $\Delta\epsilon^n_{HLL}$ defined by (3.2)	17 sec	681 991
coarse $\Delta\epsilon^n_{FD}$ defined by (3.3)	0.02 sec	634

reference results. The dose results obtained with the numerical schemes described in Section 2.1 are plotted in Fig. 7. Table 1 gathers the computation times using the different schemes.

The FD scheme with a worse $\Delta\epsilon^n_{FD}$ shows good agreement with the one with a fine $\Delta\epsilon^n_{HLL}$ (i.e. with HLL scheme). One can only see a small error appearing at the end of the medium. This error is due to the number of discontinuities of densities. This error reduces when working on media with less discontinuities. All the voxels are within 3% or 3mm distance-to-agreement, i.e. at each point x_l, whether the error is lower than 3% of the maximum dose or the dose obtained with a coarse $\Delta\epsilon^n_{FD}$ is also obtained with a fine $\Delta\epsilon^n_{HLL}$ in a radius of less than 3mm around the position x_l. As expected, the FD scheme with a coarse mesh is much faster than the one with a fine one (between 2 and 3 orders of magnitude faster). This corresponds to the different orders of magnitude between the energy step $\Delta\epsilon^n$ when using HLL scheme or FD scheme. Indeed the ratio of the different $\Delta\epsilon^n$ is $\Delta\epsilon^n_{HLL}/\Delta\epsilon^n_{FD} \approx \rho_{water}/\rho_{air} = 1000$.

3.2 2D heterogeneous medium

The following test case was used in [11] to compare the HLL scheme with a Monte Carlo simulation. We consider a domain of size $L_x = 22.3\text{cm} \times L_y = 29.5\text{cm}$, meshed with $223\times$

295 cells. The density in this medium corresponds to a 2D cut of a human chest.

We apply a beam modeled by the following boundary conditions

$$(\psi^0,\psi^1)(x=22.3cm,y,\Omega,\epsilon)=10^{10}\exp\left(-\frac{1}{2}\left(\frac{\epsilon_0-\epsilon}{0.05\epsilon_0}\right)^2\right)\exp\left(-100\left(y-\frac{L_y}{2}\right)^2\right)\alpha_\mu.$$

Here $\alpha_\mu=(1,\psi^1/\psi^0)$. We choose $\psi^1/\psi^0=(-0.98,0)$, it corresponds to an irradiation of the spinal cord. For this test case, $\epsilon_0=15MeV/m_ec^2$. We fix the initial data and the other boundary values with

$$(\psi^0,\psi^1)=(10^{-20},0,0).$$

We compare the solution using a fine energy step (HLL scheme) and a coarse one

$$\Delta\epsilon^n_{HLL}=0.95S^n\left(\frac{1}{\rho_{air}\Delta x}+2T^n\right)^{-1},\quad \Delta\epsilon^n_{FD}=0.95S^n\left(\frac{1}{\rho_{water}\Delta x}+2T^n\right)^{-1}$$

using cartesian (2.22), diagonal (2.23) and star (2.24) directions of relaxation. The isodose curves obtained are represented on Fig. 8 in colour over the chest density (grayscale).

The isocurves of absolute error induced by the extension of the stencil normalized by the maximum dose are shown on Fig. 9.

The shape of the dose obtained with the different relaxation parameters with a coarse $\Delta\epsilon^n_{FD}$ are very close to the one obtained with the cartesian relaxation parameters and a fine $\Delta\epsilon^n_{HLL}$ (HLL scheme). The absolute error is smaller than 1.1% of the maximum dose when using the cartesian set, smaller than 4.3% with the diagonal set, and smaller than 2.1% with the star set. The maximum errors are located in the middle of the medium at about 2 cm and 6 cm depth. All the voxels are within 3% or 3mm distance-to-agreement for each choice of relaxation parameters. When using the diagonal directions of relaxation, the information is transported in diagonal direction. Then, when transporting particles along the x-axis, the scheme does not transport them from one cell to its neighbour. This results in some irregularities which can be seen in Fig. 9. The relaxed models are better when the directions of relaxation are collinear to the mesh directions (i.e. cartesian directions).

The computation times for this test case are gathered in Table 2.

Table 2: Computation times for the 2D case with the different schemes.

numerical approach	computation time	number of iterations
Fine $\Delta\epsilon^n_{HLL}$ with cartesian relaxation	$\approx$ 50 min	146 224
Coarse $\Delta\epsilon^n_{FD}$ with cartesian relaxation	6.69 sec	460
Coarse $\Delta\epsilon^n_{FD}$ with diagonal relaxation	7.35 sec	460
Coarse $\Delta\epsilon^n_{FD}$ with star relaxation	19.72 sec	919

The numerical schemes presented in this paper are significantly faster than the standard method and gives precise results.

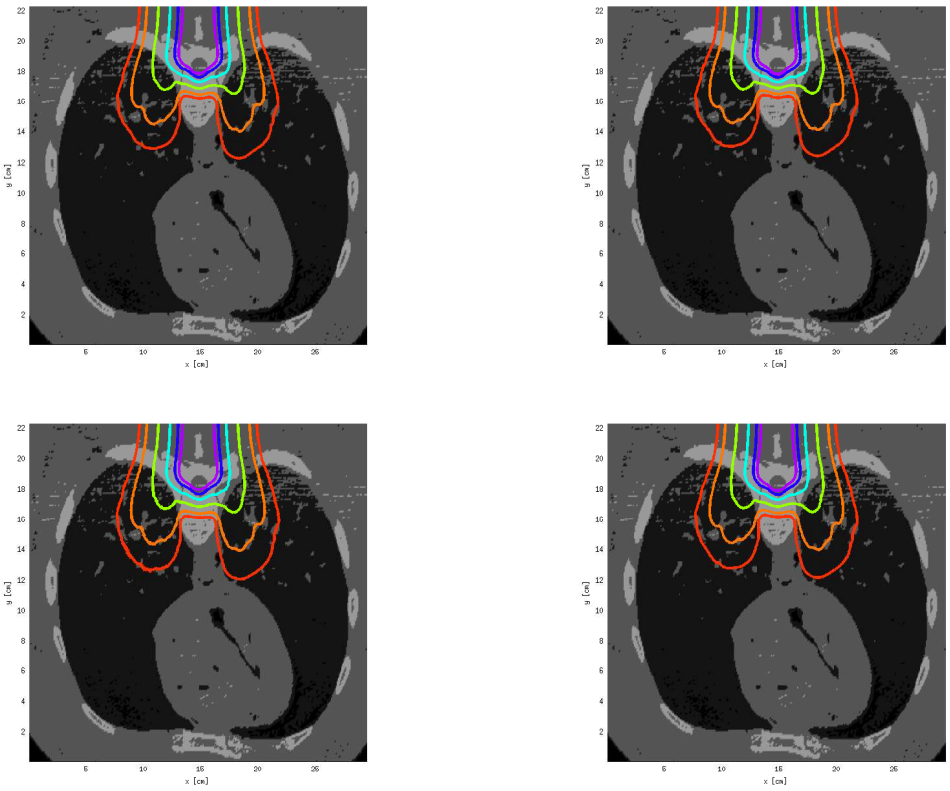

Figure 8: Isodose curves in a chest at 5% (red), 10% (orange), 25% (yellow), 50% (light blue), 70% (dark blue) and 80% (violet) of the maximum dose with a fine $\Delta\epsilon^n$ (top left) and a coarse $\Delta\epsilon^n$ using cartesian (top right), diagonal (below left) and star (below right) directions of relaxation.

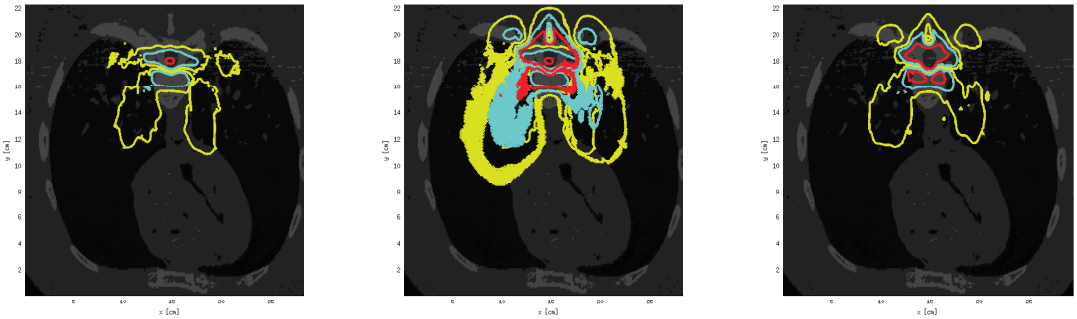

Figure 9: Isocurves of the absolute error between the doses obtained using a fine and a coarse energy step with cartesian (left), diagonal (middle) and star (right) directions of relaxation at 1% (red), 0.5% (light blue) and 0.2% (yellow) of the maximum dose.

4 Conclusion and perspective

We have proposed a numerical method for solving the M_1 system of equations applied to radiotherapy dose calculation, which is not constrained by stability restrictions. Using the method of characteristics, we proposed an unconditionally stable numerical scheme for hyperbolic systems. Then, we relax the M_1 system, which leads to a hyperbolic system of equations with linear flux terms on which we can apply the unconditionally stable numerical scheme. This method has been tested on relevant test cases and provides good results compared to the ones with the HLL scheme, and with a much smaller computational time, as we do not need to impose small energy steps.

We proposed simple sets of relaxation parameters that equals the HLL scheme in the standard case (i.e. using the mesh directions as relaxation directions and with a common CFL condition), although a general strategy to choose those parameters needs to be found.

References

[1] D. Aregba-Driollet and R. Natalini. Discrete kinetic schemes for multidimensional systems of conservation laws. *SIAM J. Numer. Anal.*, 6:1973–2004, 2000.

[2] D. Aregba-Driollet, R. Natalini, and S. Tang. Explicit diffusive kinetic schemes for nonlinear degenerate parabolic systems. *Math. Comp.*, 73:63–94, 2004.

[3] C. Berthon, P. Charrier, and B. Dubroca. An HLLC scheme to solve the M_1 model of radiative transfer in two space dimensions. *Journal of Scientific Computing*, 31(3):347–389, 2007.

[4] C. Berthon, M. Frank, C. Sarazin, and R. Turpault. Numerical methods for balance laws with space dependent flux: application to radiotherapy dose calculation. *Commun. Comput. Phys.*, 10(5), 2011.

[5] L. Boltzmann. Über die mechanische Bedeutung des zweiten Hauptsatzes der Wärmetheorie. *Wien. Ber.*, 53:195–220, 1866.

[6] F. Bouchut. Construction of BGK models with a family of kinetic entropies for a given system of conservation law. *J. Stat. Phys.*, 95(1-2):113–170, 1999.

[7] F. Bouchut. *Nonlinear stability of Finite Volume methods for hyperbolic conservation laws and well-balanced schemes for sources*. Birkhäuser, 2004.

[8] F. Bouchut, F. R. Guarguaglini, and R. Natalini. Diffusive BGK approximations for nonlinear multidimensional parabolic equations. *Indiana Univ. Math. J.*, 49:723–749, 2000.

[9] B. Dubroca and J.L. Feugeas. Hiérarchie des modèles aux moments pour le transfert radiatif. *C.R. Acad. Sci. Paris*, 329:915–920, 1999.

[10] R. Duclous, B. Dubroca, F. Filbet, and V.T. Tikhonchuk. High order resolution of the Maxwell-Fokker-Planck-Landau model intended for ICF applications. *J. Comp. Phys*, 228:5072–5100, August 2009.

[11] R. Duclous, B. Dubroca, and M. Frank. A deterministic partial differential equation model for dose calculation in electron radiotherapy. *Phys. Med. Biol.*, 55:3843–3857, July 2010.

[12] M. Falcone and R. Ferretti. Semi-lagrangian schemes for Hamilton-Jacobi equations, discrete representation formulae and Godunov methods. *J. Comp. Phys.*, 175(2):559–575, January 2002.

[13] A. Harten, P. Lax, and B. Van Leer. On upstream differencing and gudonov-type schemes for hyperbolic conservation laws. *SIAM Review*, 25(1):35–61, 1983.
[14] C. Hauck and R. McClarren. Positive P_N closures. *SIAM J. Sci. Comput.*, 32(5):2603–2626, 2010.
[15] E. T. Jaynes. Information theory and statistical mechanics. *Phys. Rev.*, 106(4):620–630, 5 1957.
[16] D. Kershaw. Flux limiting nature's own way. 1976.
[17] E. W. Larsen and G. C. Pomraning. The P_N theory as an asymptotic limit of transport theory in planar geometry I: Analysis. *Nucl. Sci. Eng.*, 109(1):49–75, september 1991.
[18] C. D. Levermore. Relating eddington factors to flux limiters. *J. Quant. Spectrosc. Radiat. Transfer*, 31(2):149–160, 1984.
[19] C. D. Levermore. Moment closure hierarchies for kinetic theories. *J. Stat. Phys.*, 83(5–6):1021–1065, June 1996.
[20] J. Mallet, S. Brull, and B. Dubroca. An entropic scheme for an angular moment model for the classical Fokker-Planck-Landau equation of electrons. *Commun. Comput. Phys.*, 15(2):422–450, 2014.
[21] J. Mallet, S. Brull, and B. Dubroca. General moment system for plasma physics based on minimum entropy principle. submitted.
[22] G. N. Minerbo. Maximum entropy eddington factors. *J. Quant. Spectros. Radiat. Transfer*, 20:541–545, 1978.
[23] Roberto Natalini. A discrete kinetic approximation of entropy solutions to multidimensional scalar conservation laws. *J. diff. eqns*, 148(2):292–317, 1998.
[24] G. C. Pomraning. *The equations of radiation hydrodynamics*. Pergamon Press, 1973.
[25] G. Russo and F. Filbet. Semilagrangian schemes applied to moving boundary problems for the BGK model of rarefied gas dynamics. *Kinetic and Related Models*, 2(1):231–250, 2009.
[26] E.F. Toro. *Riemann solvers and numerical methods for fluid dynamics*. Springer, 1999.